Topics in Catalysis (2020) 63:895–912
https://doi.org/10.1007/s11244-020-01317-9

ORIGINAL PAPER

Photocatalytic Production of Hydrogen Peroxide over Modified Semiconductor Materials: A Minireview

Haiyan Song[1] · Lishan Wei[1] · Luning Chen[2] · Han Zhang[1] · Ji Su[2]

Published online: 9 July 2020

Abstract
Hydrogen peroxide (H_2O_2) has exhibited huge application value in many fields including chemical synthesis, medicine, environmental remediation, and fuel cells. Traditional anthraquinone method for H_2O_2 commercial production has emerged the drawbacks of toxicity, H_2 consumption and high energy input. Photocatalytic production of H_2O_2, which only requires water, oxygen, solar light and catalyst, is a novel and green technique, and potentially becomes one of the substitutes for anthraquinone method. Herein, we comprehensively review the research progress in the reported semiconductor catalysts, their modification strategies, as well as the related photocatalysis systems and mechanisms for the light driven H_2O_2 production. In detail, the photocatalysts are introduced from different families including ZnO, g-C_3N_4, TiO_2, metal complexes, metal sulfides, Bi containing semiconductors, and carbon materials. In the meantime, their modification strategies are systematically evaluated aiming at the improvement in the structures and the photoelectrical properties of semiconductors, as well as their effective activation of molecular O_2, and inhibition of H_2O_2 decomposition. Finally, this review is concluded with a brief summary and outlook, and the major challenges for the development of photocatalytic H_2O_2 production over the emerging semiconductor photocatalysts.

Keywords Hydrogen peroxide · Photocatalysis · Oxygen reduction · Semiconductors · Modification

1 Introduction

Hydrogen peroxide (H_2O_2) is a green and efficient oxidant, which can oxidize various inorganic and organic substrates in liquid-phase reactions under very mild conditions, and generates only one clean byproduct of water (H_2O). H_2O_2 has been widely used in many industrial fields including chemical industry, medicine and biological process, and environmental remediation [1, 2]. Very recently, H_2O_2 is also exploited to be a potential energy carrier for fuel cells [3–5]. H_2O_2 exhibits several advantages to become an alternative to H_2 fuel cells: (1) H_2O is the only and clean byproduct in fuel cells; (2) the liquid state of H_2O_2 makes it more convenient and safer in storage and transportation; (3) it can be made into a fuel cell of single-compartment with more simplification and better scales than that of H_2 two-compartment.

H_2O_2 production of industrial scale has been achieved via the anthraquinone oxidation (AO) process [6, 7]. However, anthraquinone oxidation is a multistep method that contains hydrogenation, oxidation and extraction procedures in organic solvents, requiring high energy input and emitting a lot of wastes [7, 8]. Therefore, the AO method aggravates the difficulty and hazards in transport and storage, and hardly satisfies the demands for green production and the cost efficiency. Other alternative methods, such as alcohol oxidation and electrochemical synthesis have also been practiced in industrial production of H_2O_2 [6, 8, 9]. However, the purity and quality of the produced H_2O_2 via those methods is not

✉ Han Zhang
Zhanghantdcq@126.com

✉ Ji Su
jisu@lbl.gov

Haiyan Song
chem_shy@163.com

Lishan Wei
Weilishandddct5439@126.com

[1] Department of Chemistry and Chemical Engineering, College of Chemistry, Chemical Engineering and Resource Utilization, Northeast Forestry University, Harbin 150040, People's Republic of China

[2] Materials Sciences Division, Lawrence Berkeley National Laboratory, Berkeley, CA 94720, USA

as good as that via the AO process. Therefore, it is essential to develop cost-effective and eco-friendly methods for H_2O_2 production. During the last two decades, direct synthesis of H_2O_2 from hydrogen (H_2) and oxygen (O_2) in the presence of a catalyst has been regarded as another alternative approach for AO process [10–13]. The direct method is an innovation that H_2O_2 is simply synthesized from its elements by one step, and the H_2O_2 can be used in an oxidation reaction in situ. There are three major problems for the direct method: (1) inert gas (e.g. N_2, CO_2 and Ar) must be charged in order to keep away from the explosive limit of H_2/O_2 mixture; (2) the noble metals (e.g. Pd, Au and Pt), and their alloys (e.g. Pd–Au and Pd–Pt) act as the active centers on various supports, which increase the cost of catalyst; (3) some noble metals like Pd and Au are also active for the H_2O_2 decomposition, which decreases the synthesis efficiency of H_2O_2. Although the catalytic oxidation of H_2 to generate H_2O_2 has been known since 1914, this technique has not yet been put into industrial practice [14].

In recent years, H_2O_2 production from photocatalysis of semiconductors arouses much attention and is frequently reported due to the sufficient and renewable sunlight as driving force [15]. Photocatalytic production of H_2O_2 over semiconductor is at least known since the report of Baur and Neuweiler in 1927 [16]. This developing technique involves only light, water, molecular O_2 and the catalyst, which is eco-friendly, and is recommended to be applied in the field of oxidations and solar fuels demanding for a mild scale of H_2O_2. In general, the photocatalysis process involves two major half reactions: (1) two-electron reduction of O_2 from the conduction band (CB) (Eq. 1); (2) oxidation of H_2O by holes (h^+) in valence band (VB) to generate O_2 (Eq. 2). Meanwhile, there are several side reactions, which lower the H_2O_2 selectivity: (1) one-electron reduction of O_2 to generate peroxy radicals (·OOH) (Eq. 3); (2) four-electron reduction of O_2 to generate H_2O (Eq. 4). Therefore, H_2O_2 concentrations in many reported works hardly achieve the mmol/L scale due to the existence of those side reactions. In the field of photocatalytic production of H_2O_2, effective inhibition of the one-electron and the four-electron reductions of O_2 becomes the major challenge for most of the semiconductor photocatalysts. Introducing the new structures or the guest molecules to the host semiconductors is an effective strategy to promote the charge separation and increase the selectivity of the two-electron reduction of O_2 to H_2O_2. In addition, multi-channels for H_2O_2 production are possibly opened by the modified semiconductors. In another aspect, a number of works adopt molecular O_2 (pure oxygen gas) or organic electron donors (alcohols) to enhance the H_2O_2 yield, which are far away from the concept of cost-efficiency and green synthesis. Therefore, saving the pure O_2 or electron donor by using appropriate photocatalyst becomes another challenge for photocatalytic production of H_2O_2.

$$O_2 + 2H^+ + 2e^- \rightarrow H_2O_2 (0.68\ \text{V vs. NHE}) \quad (1)$$

$$H_2O + 2h^+ \rightarrow 1/2O_2 + 2H^+ (1.23\ \text{V vs. NHE}) \quad (2)$$

$$O_2 + H^+ + e^- \rightarrow {}^{\cdot}OOH\ (-0.13\ \text{V vs. NHE}) \quad (3)$$

$$O_2 + 4H^+ + 4e^- \rightarrow H_2O\ (1.23\ \text{V vs. NHE}) \quad (4)$$

So far, the reported catalysts for photocatalytic production of H_2O_2 can be classified as graphitic carbon nitride (g-C_3N_4) [15, 17–27], TiO_2 [28–33], transition metal sulfide [34–38], $BiVO_4$ [39], transition metal complexes [40–44] and organic ions [45, 46] based materials. In this minireview, we mainly aim at the recent advances and challenges associated with the photocatalytic H_2O_2 production, as well as the related semiconductor photocatalysts. It contains the preparation of semiconductors, the modification strategies, and the related mechanism of H_2O_2 production over the semiconductors.

2 Photocatalytic Production of H_2O_2 over g-C_3N_4 Based Materials

So far, the reports on g-C_3N_4 as fundamental catalysts for light-driven H_2O_2 production are rapidly increasing in number. G-C_3N_4, consisting of earth-abundant elements only, and possessing 2.7 eV of band gap and graphene-like 2D morphology, has been regarded as an appealing and potential photocatalyst. The conduction band of g-C_3N_4 (− 1.3 V vs. NHE) is suitably located to facilitate O_2 reduction (− 0.28 V vs. NHE), and its lower valence band potential (1.4 V vs. NHE) can prevent the oxidative decomposition of H_2O_2. Many efforts have been made for g-C_3N_4 to solve the problems of the fast charge recombination caused intrinsically by the π–π conjugated electronic system of g-C_3N_4 framework, and the limited inhibition of the one-electron reduction of O_2.

2.1 Single C_3N_4 Photocatalysts

Fabrication of a single C_3N_4 photocatalyst is a simple and low-cost way to enhance the photocatalytic performance. The single C_3N_4 photocatalyst can be fabricated based on the preparation of pristine g-C_3N_4 without adding or doping other species. After the treatments of instruments or chemical reagents, the photocatalysts can achieve the improvements in their frameworks, pores and surface, crystal structure, or photoelectric properties to increase the H_2O_2 productivity.

One of the strategies is to fabricate the g-C_3N_4 of appropriate morphology without changing its intrinsic molecule or

crystal structure. Shiraishi et al. earlier used the metal-free polymeric photocatalyst g-C_3N_4 for photocatalytic production of H_2O_2 (Fig. 1a) [20, 47]. They found that g-C_3N_4 with alcohol and O_2 can selectively promote the two-electron reduction of O_2 due to the efficient formation of 1,4-endoperoxide species on its surface, while suppressed the subsequent decomposition of the formed H_2O_2. In addition, the g-C_3N_4 catalyst activated by visible light can oxidize water owing to the positively shifted VB levels, while maintaining high selectivity for two-electron reduction of O_2. This thus facilitated highly efficient production of H_2O_2 with more than 90% selectivity. In order to improve the catalytic activity and the H_2O_2 selectivity of g-C_3N_4, the same group subsequently reported a mesoporous g-C_3N_4 prepared by silica-templated thermal polymerization of cyanamide for photocatalytic production of H_2O_2 [25]. Mesoporous g-C_3N_4 with larger surface area contained primary amine groups on the surface, which decreased the H_2O_2 selectivity and increased the photocatalytic decomposition of the formed H_2O_2. Selectivity for H_2O_2 formation via two-electron reduction of O_2 by the conduction band electrons localized on the 1,4-positions of the melem unit decreased with an increase in the surface area. Therefore, H_2O_2 productivity was adjusted by the surface area and the surface defects of mesoporous g-C_3N_4 (Fig. 1b–d). Ou et al. developed a self-assembly method to prepare a self-supported C_3N_4 aerogel with large surface area, incorporated functional groups and 3D network structure [48]. The C_3N_4 aerogel obtained high photocatalytic activity for hydrogen evolution and H_2O_2 photoproduction.

Another strategy is to improve the photoelectric properties of g-C_3N_4 by introduction of vacancies or displacement of atoms. Carbon vacancies method was adopted to modulate g-C_3N_4 with an improvement in electrons transfer and band gap [49]. H_2O_2 generation pathway could be changed from a two-step single-electron indirect reduction to the one-step two-electron direct reduction by the carbon vacancies in g-C_3N_4. Therefore, photoproduction of H_2O_2 was improved by 14 times in the absence of organic scavenger through the carbon vacancy-based strategy. A reduced g-C_3N_4 material was prepared by a thermal treatment with $NaBH_4$ in N_2 atmosphere [18]. The reduction treatment created nitrogen vacancies followed by a formation of functional group C≡N (Fig. 2), which endowed g-C_3N_4 with a feature of visible light-driven water oxidation capacity. In addition, the reduction treatment facilitated the spatial separation of photo-excited electron and hole, and enhanced the charge transfer. Therefore, an optimal reduced g-C_3N_4 obtained enhanced performance in photocatalytic production of H_2O_2 (170 μmol/L h^{-1}) from pure H_2O and O_2 at ambient atmosphere in the absence of organic electron donors. A parent g-C_3N_4 was treated with a dielectric barrier discharge (DBD) plasma, and a PT-g-C_3N_4 material for photocatalytic production of H_2O_2 was finally obtained [50] (Fig. 3a). Compared with bare g-C_3N_4, PT-g-C_3N_4 improved the grain size, the surface and pore properties, as well as

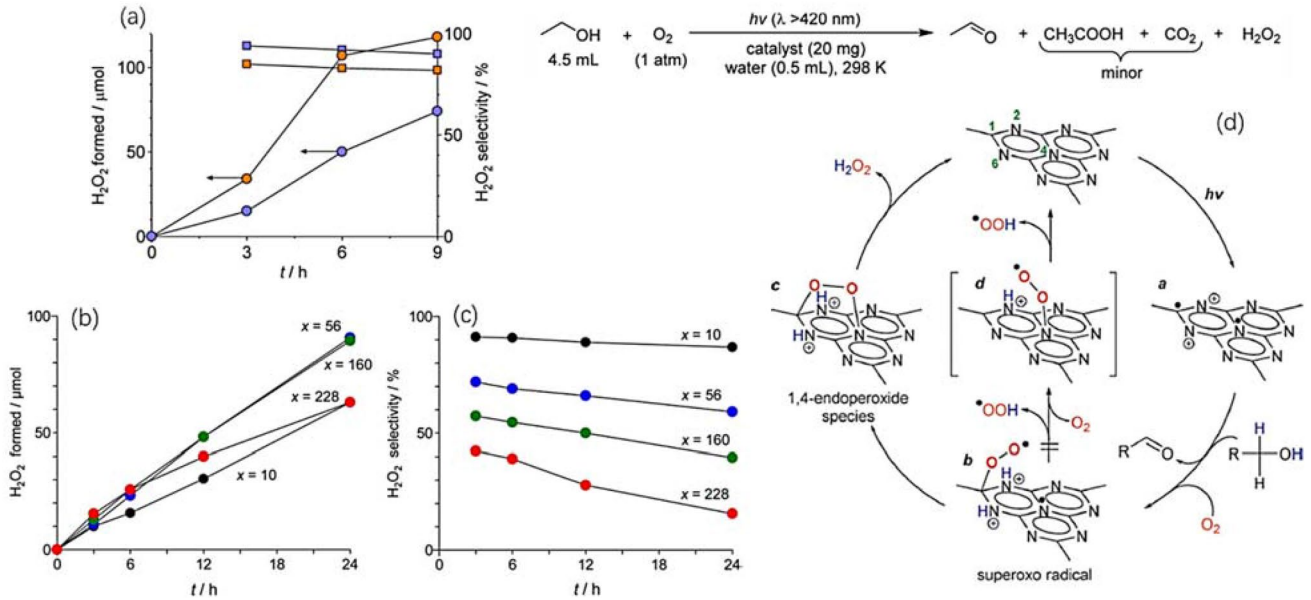

Fig. 1 Amount and selectivity of H_2O_2 over g-C_3N_4 in a 2-propanol/water/O_2 system under sunlight exposure (orange) without filter and (blue) with filter (λ > 420 nm) (**a**) [20], copyright 2014 American Chemical Society; amount (**b**) and selectivity (**c**) of H_2O_2 over mesoporous g-C_3N_4 with different surfaces areas (*x*, m^2 g^{-1}) [25], copyright 2015 American Chemical Society; pathway of selective H_2O_2 production on g-C_3N_4 under visible light irradiation (**d**) [25], copyright 2015 American Chemical Society

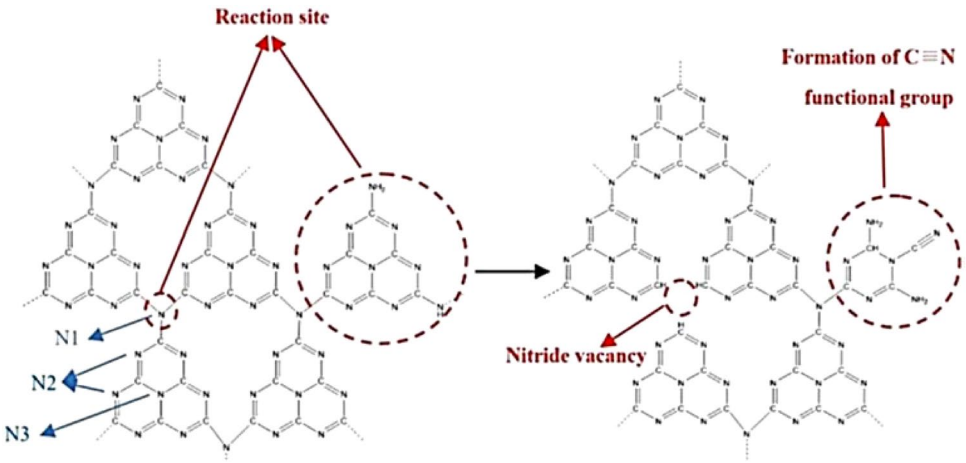

Fig. 2 Probable reaction of g-C_3N_4 treated with $NaBH_4$ [18], copyright 2018 Elsevier

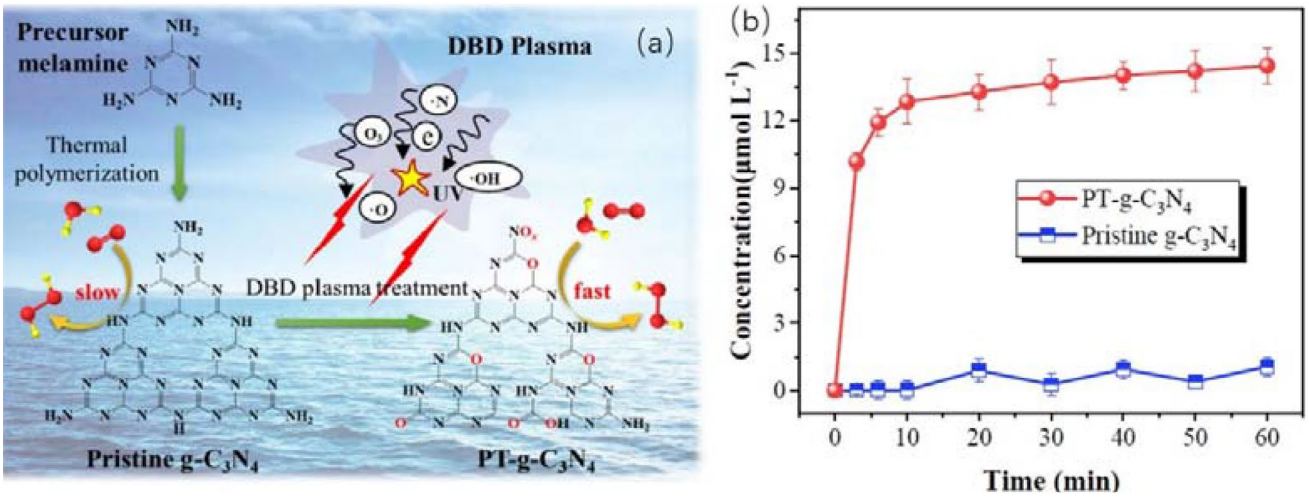

Fig. 3 Mechanism illustration of DBD plasma introducing oxygen-containing functional groups on the surface of g-C_3N_4 (**a**) [50], copyright 2020 Elsevier; photocatalytic activity of pristine g-C_3N_4 and PT-g-C_3N_4 for photocatalytic production of H_2O_2 (**b**) [50], copyright 2020 Elsevier

the hydrophilic property. Furthermore, PT-g-C_3N_4 significantly improved the H_2O_2 yield by 13 times based on pristine g-C_3N_4 (Fig. 3b).

2.2 Modified g-C_3N_4 Photocatalysts

Introducing the guest molecules or semiconductors to g-C_3N_4 host is effective and frequently used to promote the charge separation and the selectivity of the two-electron reduction of O_2 to H_2O_2. Moreover, the bandgap of g-C_3N_4 is easily modulated by doping, hybridization or surface decoration, which can promote the effective utilization of visible light [21]. The introduced species mainly include hetero-elements, nanoparticles, semiconductors, organic compounds, polymers. The modification strategies, photocatalytic performances and properties of the reported g-C_3N_4 based materials for photocatalytic H_2O_2 production are collected in Table 1.

2.2.1 Elements Doping

Incorporation of earth-abundant heteroelements (K, P or O) can efficiently improve the crystal structure and the band gap of g-C_3N_4 to enhanced its photocatalytic performance. An in situ incorporation of both potassium and phosphate species into the polymeric C_3N_4 framework was reported [51]. The incorporated K, P and O species introduced the negative surface charge, facilitated the interfacial electron transfer to dioxygen, and inhibited the decomposition of in situ generated H_2O_2. Therefore, the modified C_3N_4 enhanced the apparent quantum yields of H_2O_2 by about 25 and 17 times under monochromatic irradiation of 420 and 320 nm, respectively (Fig. 4a). The high selectivity

Table 1 Summary of the modification strategies, photocatalytic performances and properties of the reported g-C_3N_4 based materials for photocatalytic H_2O_2 production

Photocatalyst	Modification strategy	Reaction system	H_2O_2 productivity	References
g-C_3N_4	Pristine	Visible light; 5 mL Alcohol/water; O_2	30 μmol (24 h)	[20]
g-C_3N_4/PDI	Mixture heating	Visible light; 50 mL Water; O_2	50.6 μM (48 h)	[47]
Mesoporous g-C_3N_4	Silica-templated thermal polymerization	Visible light; 5 mL EtOH/water; O_2	90 μmol (24 h)	[25]
C_3N_4 aerogel	Self-assembly	Visible light; 30 mL water; O_2	36 μmol (25 h)	[48]
g-C_3N_4	Carbon vacancy-based strategy	Visible light; 100 mL water; O_2	~90 μM (1 h)	[49]
Reduced g-C_3N_4	Thermal treatment with $NaBH_4$	Visible light; 100 mL water; O_2	170 μM (1 h)	[18]
g-C_3N_4	Dielectric barrier discharge plasma modification	Visible light; 60 mL water	27 μM (1 h)	[50]
K, P, O-C_3N_4	Calcination with K_2HPO_4	Visible light; 40 mL EtOH/water; O_2	1.7 mM (7 h)	[51]
KPF_6-C_3N_4	Thermal polymerization	Visible light; EtOH/water; O_2	1.5 mM (5 h)	[27]
Hollow Cu-doped g-C_3N_4	Template method	Visible light; 200 mL water; 80 mL/min of O_2 bubbling	4.5 mM (4 h)	[23]
Au/C_3N_4	KBH_4 reduction	Visible light; 100 mL EtOH/water (pH 8.5); O_2	2 mM (30 h)	[55]
BNQDs/UPCN	Two steps	Visible light; 50 mL isopropanol/water; O_2	74 μM (1 h)	[56]
3DOM g-C_3N_4-PW_{11}	Covalent combining and organic linker strategy	Visible light; 100 mL water; O_2	14.4 μmol (6 h)	[22]
g-C_3N_4-CoWO	Precursor co-calcination	Visible light; 100 mL water; O_2	9.7 μmol (1 h)	[59]
PI-NCN	Gas soft-template and condensation reaction method	Visible light; 50 mL water	124 μmol (2 h)	[17]
C-N-g-C_3N_4	Living Chlorella vulgaris and carbon micro particle modification	Visible light; 15 mL water; O_2	12.1 μmol (12 h)	[60]
g-C_3N_4-CNTs	Amidation reaction	Visible light; 100 ml of formic acid/water; O_2	53.8 μmol (4 h)	[26]
$Cu_2(OH)PO_4$/g-C_3N_4	Hydrothermal and co-calcination	Simulated solar light source; 200 mL water; 80 mL/min of O_2 bubbling	8.9 mM (18 h)	[61]
Ti_3C_2/porous g-C_3N_4	Electrostatic self-assembly route	Visible light; 50 mL isopropanol/water; O_2	131.71 μmol (1 h)	[62]

toward H_2O_2 over H_2 are attributed to the enhanced light absorption, the increased lifetime of the transient species, the effective interfacial charge transfer to dioxygen, and the inhibited decomposition of in situ generated H_2O_2 (Fig. 4b). Later, the same group incorporated the potassium hexafluorophosphate into the C_3N_4 structure to obtain a composite photocatalyst (KPF_CN) [27]. Compared with C_3N_4, the introduction of KPF_6 could increase the absorption of visible light, the charge carrier density and the selective two-electron transfer to O_2, and inhibit the photodecomposition of H_2O_2. The catalyst greatly enhanced the apparent quantum yield of H_2O_2 (26.1 times higher than that of bare C_3N_4) in visible light region (Fig. 4c). The high selectivity for O_2 reduction in KPF_CN attributes to the optimized interactions of O_2 molecules and protons with K^+ and PF_6 sites, respectively. A series of potassium and phosphorus doped g-C_3N_4 catalysts for H_2O_2 photoproduction was synthesized and reported (Fig. 4d) [52]. The optimal catalyst achieved 5 mM of H_2O_2 for 10 h, which were 5 folds of that over pure g-C_3N_4. Xue et al. prepared a Co_xNi_yP cluster incorporated P-doped g-C_3N_4 (Co_xNi_yP-PCN) photocatalyst by a two-step phosphating method [53] (Fig. 5a–c). It was found that P as a substitution of C in g-C_3N_4 introduced a positive charge center (P^+) forming a unique bridging effect. The bridging effect with the extended light absorption by P doping and optimized surface redox potential by cocatalyst integration stimulated efficient vectorial charge transfer between PCN and CoNiP and subsequent surface mass exchange (Fig. 5d). As a result, the two-electron reaction pathway for H_2O_2 photogeneration was facilitated.

In addition, Hu's group prepared a hollow Cu doped g-C_3N_4 microspheres, in which Cu species was inserted at the interstitial position through the coordinative Cu(I)-N bonds [23]. With a self-established system (Fig. 6a) for H_2O_2 photoproduction, the Cu doped g-C_3N_4 displayed higher H_2O_2 productivity (4.8 mM) and better structural stability than neat g-C_3N_4. With the aid of DFT simulation (Fig. 6b, c), they concluded that the Cu(I)–N active sites could activate molecular O_2, and built an "electron transfer bridge" to the adsorbed O_2 molecules.

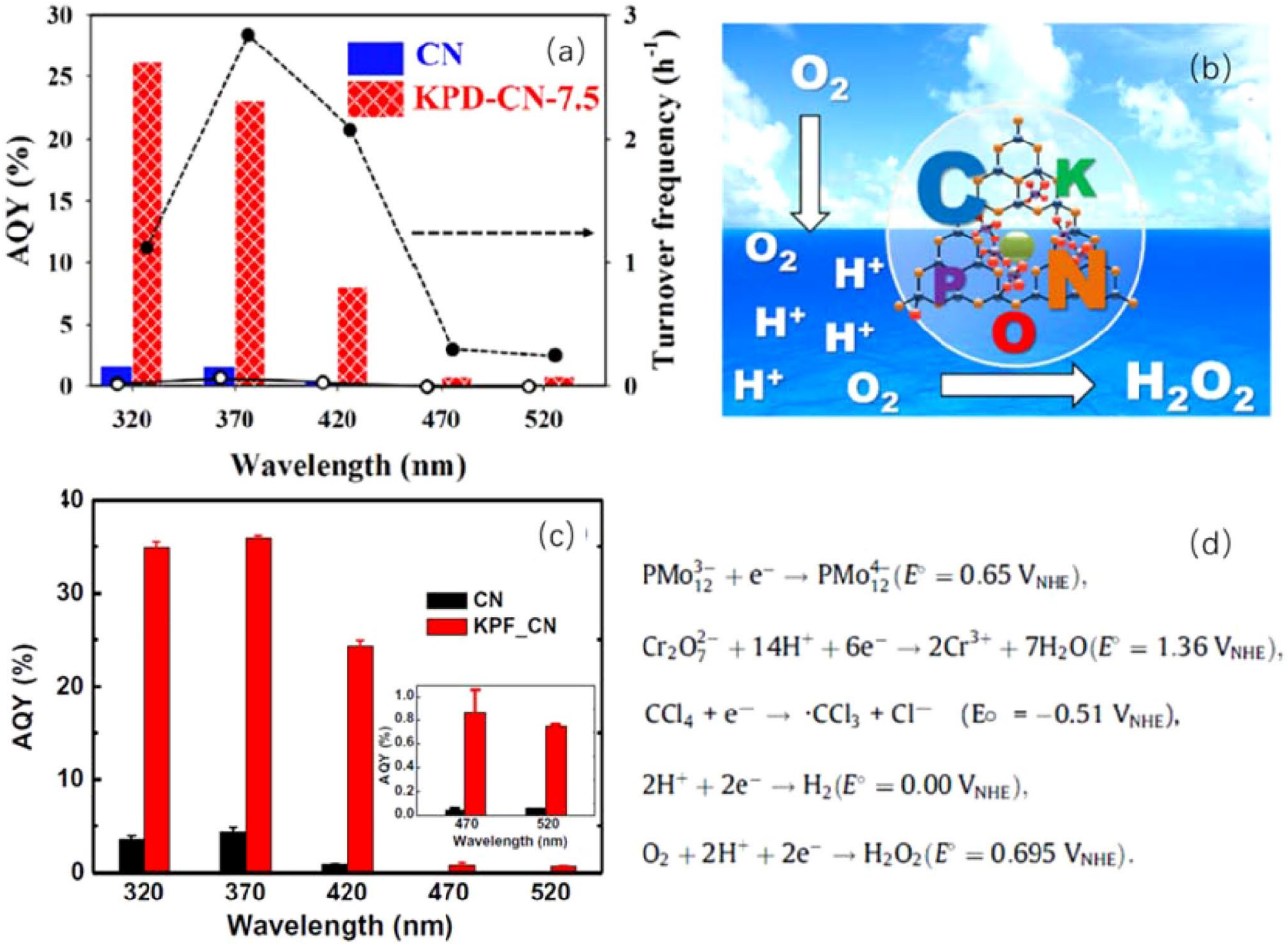

Fig. 4 Apparent quantum yield of H_2O_2 photoproduction over KPD-CN (**a**) and the O_2 activation pathway (**b**) [51], copyright 2017 American Chemical Society; apparent quantum yield of H_2O_2 photoproduction over KPF_CN (**c**) and the O_2 activation pathway (**d**) [27], copyright 2018 Elsevier

2.2.2 Surface Decoration

Surface modification with functional species or supporting nanoparticles on the parent photocatalyst is an efficient approach to improve the photocatalytic activity by promoting the charge separation and selectively catalyzing relevant reactions. The enhancement effect of Au nanoparticles for H_2O_2 generation has been demonstrated over the TiO_2 photocatalysts [54]. Thereby, Zuo et al. carried out photocatalytic production of H_2O_2 over g-C_3N_4 supporting Au nanoparticles [55]. Au nanoparticles showed inert nature for the decomposition of H_2O_2, and thus increased the H_2O_2 yield. A boron nitride quantum dots modified ultrathin porous g-C_3N_4 (BNQDs/UPCN, BU) composite was constructed via two steps [56] (Fig. 7a, b). The superoxide radical ($\cdot O^{2-}$) generation rate over the composite was estimated to be 2.3 times higher than that over bulky g-C_3N_4 (Fig. 7c), owing to that the composite simultaneously promoted the dissociation of excitons and accelerate the transfer of charges (Fig. 7d).

Polyoxometalates (POMs) are classified as metal–oxygen cluster compounds, which can act as electron reservoirs and exhibit extensive ranges of structures and stable redox states [57]. In particular, POMs contain several empty *d* orbitals that allow them to accept electrons without causing a structural change. These compounds also have nucleophilic oxygen-enriched surfaces and multi-hydrogen protons [58]. Zhao's group prepared a photocatalyst (3DOM g-C_3N_4) by the covalent combination of a polyoxometalate cluster of $[PW_{11}O_{39}]^{7-}$ with a macroporous g-C_3N_4 through the organic linker strategy [22] (Fig. 7a). The catalyst obtained 2.4 μmol h^{-1} of light driven H_2O_2 production in the absence of organic electron donors (Fig. 7b). The positive shift of the CB in 3DOM g-C_3N_4-PW_{11} is likely to improve the selectivity of O_2 reduction to H_2O_2. Later, they prepared a hybrid catalyst of g-C_3N_4-CoWO via the calcination of the 3-amino 1,2,4-triazole and the $(NH_4)_8Co_2W_{12}O_{42}$ precursors [59] (Fig. 7c). The hybrid catalyst with well-defined and stable structure obtained 9.7 μmol h^{-1} of H_2O_2 productivity

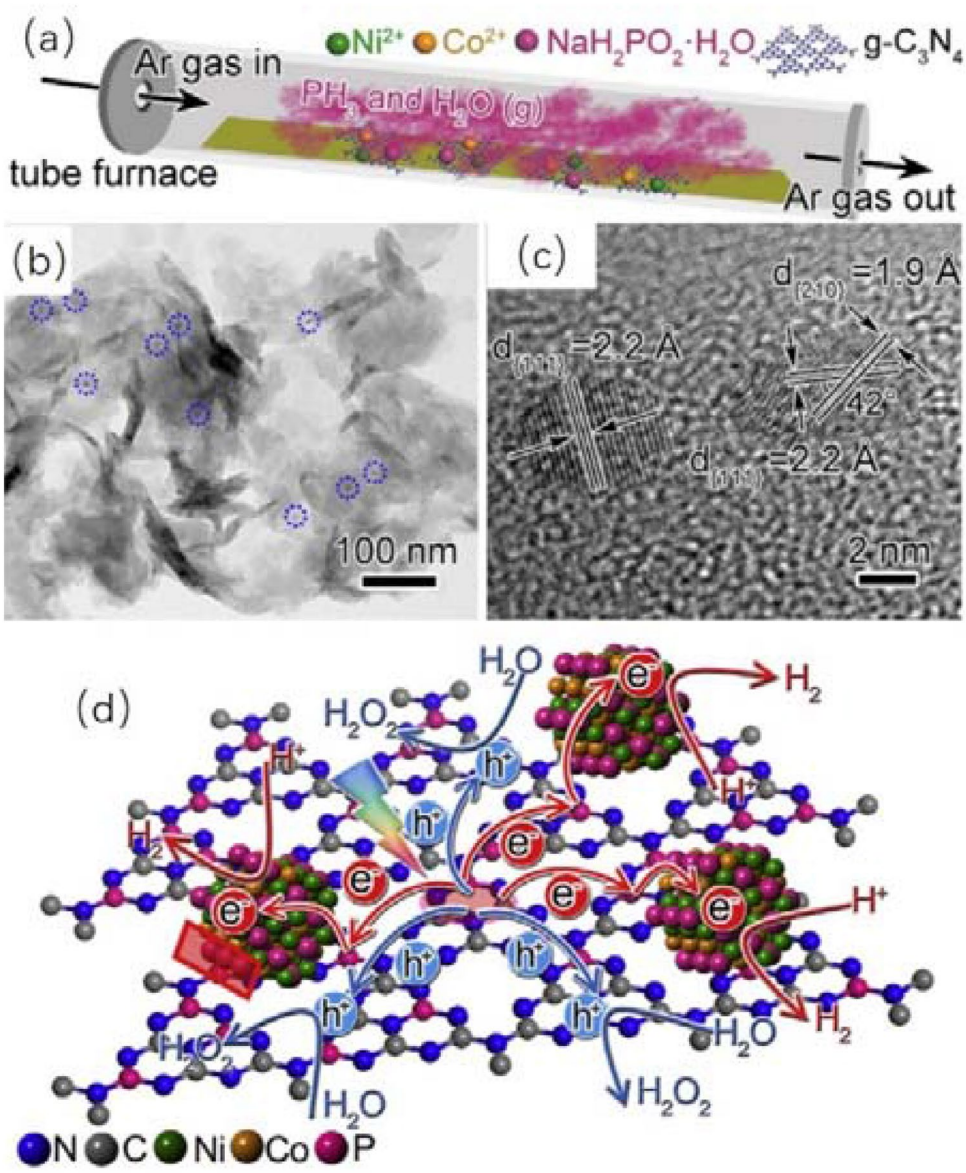

Fig. 5 Schematic illustration for preparation of CoNiP–PCN (**a**) [53], copyright 2019 Elsevier; TEM (**b**) and HRTEM (**c**) imagines of CoNiP–PCN [53], copyright 2019 Elsevier; proposed mechanism of H_2O_2 photoproduction over CoNiP–PCN (**d**) [53], copyright 2019 Elsevier

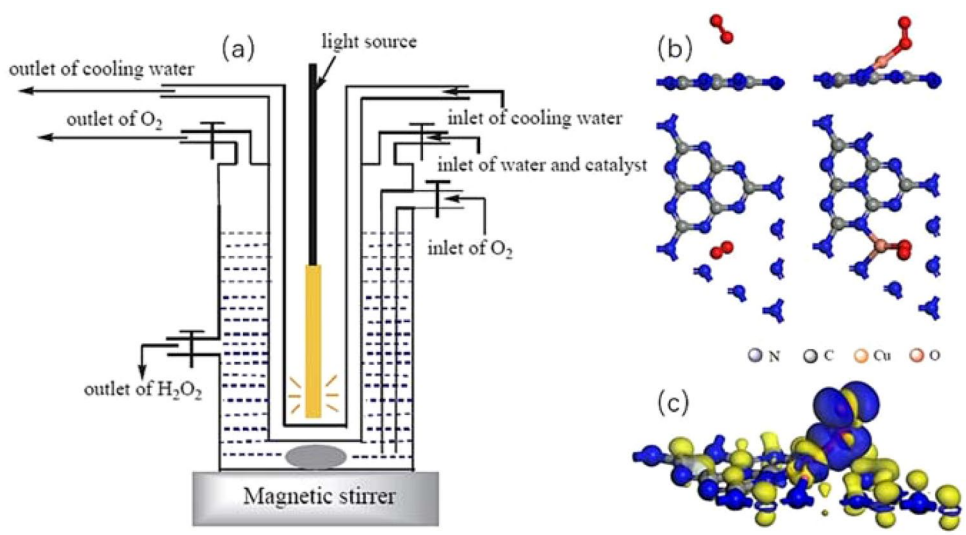

Fig. 6 Schematic diagram of photocatalytic H_2O_2 production (**a**) [23], copyright 2018 Elsevier; Optimal O_2 adsorption models on g-C_3N_4 (left) and Cu doped g-C_3N_4 (right) (**b**) [23], copyright 2018 Elsevier; charge density difference of O_2 molecule adsorbed on a Cu^+ doping site (The yellow and blue isosurfaces represent charge accumulation and depletion in the space, respectively) (**c**) [23], copyright 2018 Elsevier

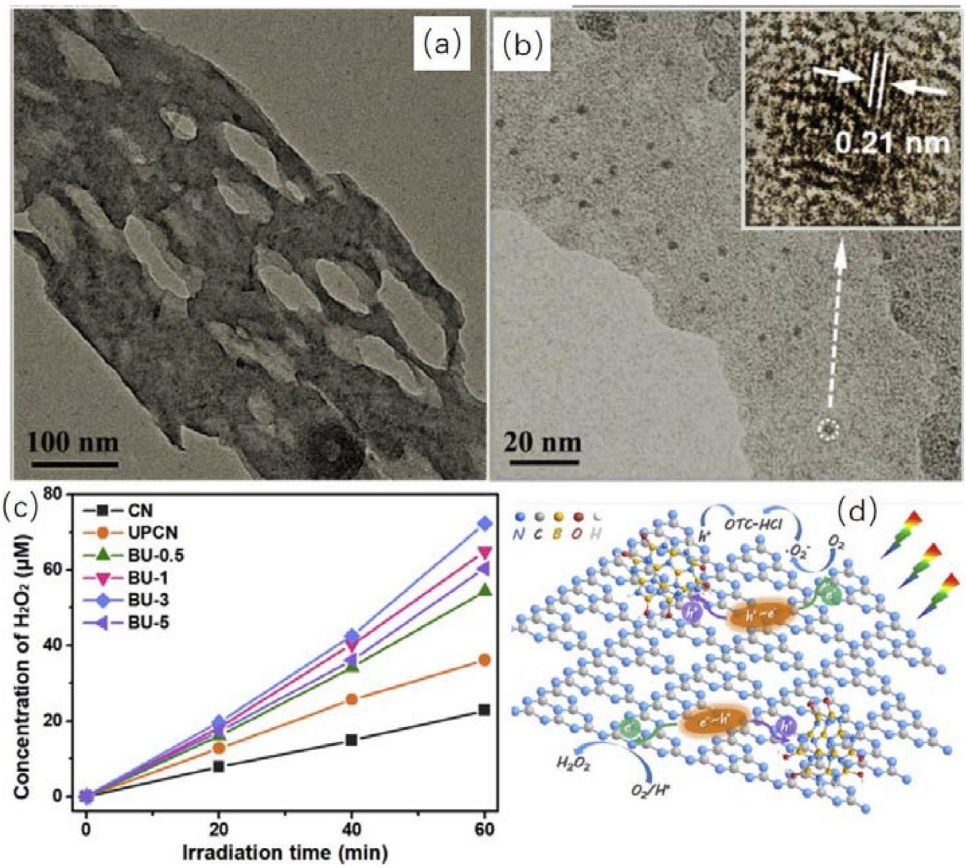

Fig. 7 TEM and HRTEM images of BNQDs/UPCN (**a**, **b**) [56], copyright 2019 Elsevier; H_2O_2 photoproduction over different BNQDs/UPCN samples (**c**) [56], copyright 2019 Elsevier; proposed photocatalytic mechanism in BNQDs/UPCN heterostructure (**d**) [56], copyright 2019 Elsevier

in the absence of organic electron donor under visible light (Fig. 7d).

Organic compounds and organisms are also practiced in photocatalytic H_2O_2 production to become good cocatalysts of g-C_3N_4. An all-solid-state Z-scheme heterojunction (PI-NCN) was constructed by assembling perylene imides (PI) on g-C_3N_4 nanosheets (NCN) via gas soft-template and condensation reaction method [17]. Electrons in conduction band of PI were transferred into the valence band of g-C_3N_4 by photoexcitation, which provided more electrons for the reduction of O_2 to generate more H_2O_2. Therefore, PI could change H_2O_2 generation from single-channel to two-channel route. Fu et al. were inspired by the behavior of chlorella as a biological H_2O_2 generator, and prepared a living chlorella vulgaris and carbon micro particle (needle coke) co-modified g-C_3N_4 (C-N-g-C_3N_4) photocatalyst [60]. The novel material achieved the simultaneous photocatalytic water splitting and biological H_2O_2 generation with H_2O_2 productivity of 0.98 μmol h^{-1} (Fig. 8).

2.2.3 Hybridization

Hybridization is a widely accepted approach to obtain an efficient and stable photocatalyst of heterojunction. A hybrid catalyst of g-C_3N_4 and carbon nanotubes (g-C_3N_4-CNTs) with well-defined and stable structure was prepared through an amidation reaction [26]. The CNTs covalent combined with g-C_3N_4 promoted the electrons generation (Fig. 9a). Therefore, the single-electron reduction of O_2 to $\cdot O_2^-$ and the sequential two-step single-electron O_2 reduction reaction was promoted successively (Fig. 9a). The hybrid catalyst obtained 32.6 μmol·h^{-1} of H_2O_2 productivity in the presence of formic acid under visible light. A $Cu_2(OH)PO_4$/g-C_3N_4 composite was prepared via the hydrothermal and co-calcination procedures for photocatalytic H_2O_2 production [61]. $Cu_2(OH)PO_4$ could adsorb O_2 molecules, and formed photogenerated electrons to recombine the holes in g-C_3N_4 through a Z-scheme mechanism. The heterojunction catalyst with 20 wt% of $Cu_2(OH)PO_4$ obtained 7.2 mM of H_2O_2, which was over 13 times higher than that of pure g-C_3N_4. An interfacial Schottky junction composed of Ti_3C_2 nanosheets and porous g-C_3N_4 nanosheets (TC/pCN) was fabricated via an electrostatic self-assembly route [62]. The formation of Schottky junction and subsequent built-in electric field at their interface accelerated the spatial charge separation and restrain the charge recombination (Fig. 9b). TC/pCN exhibited a high H_2O_2 yield (2.20 μmol L^{-1} min^{-1}) under visible light irradiation ($\lambda > 420$ nm), which is about 2.1 times higher than that of bare g-C_3N_4.

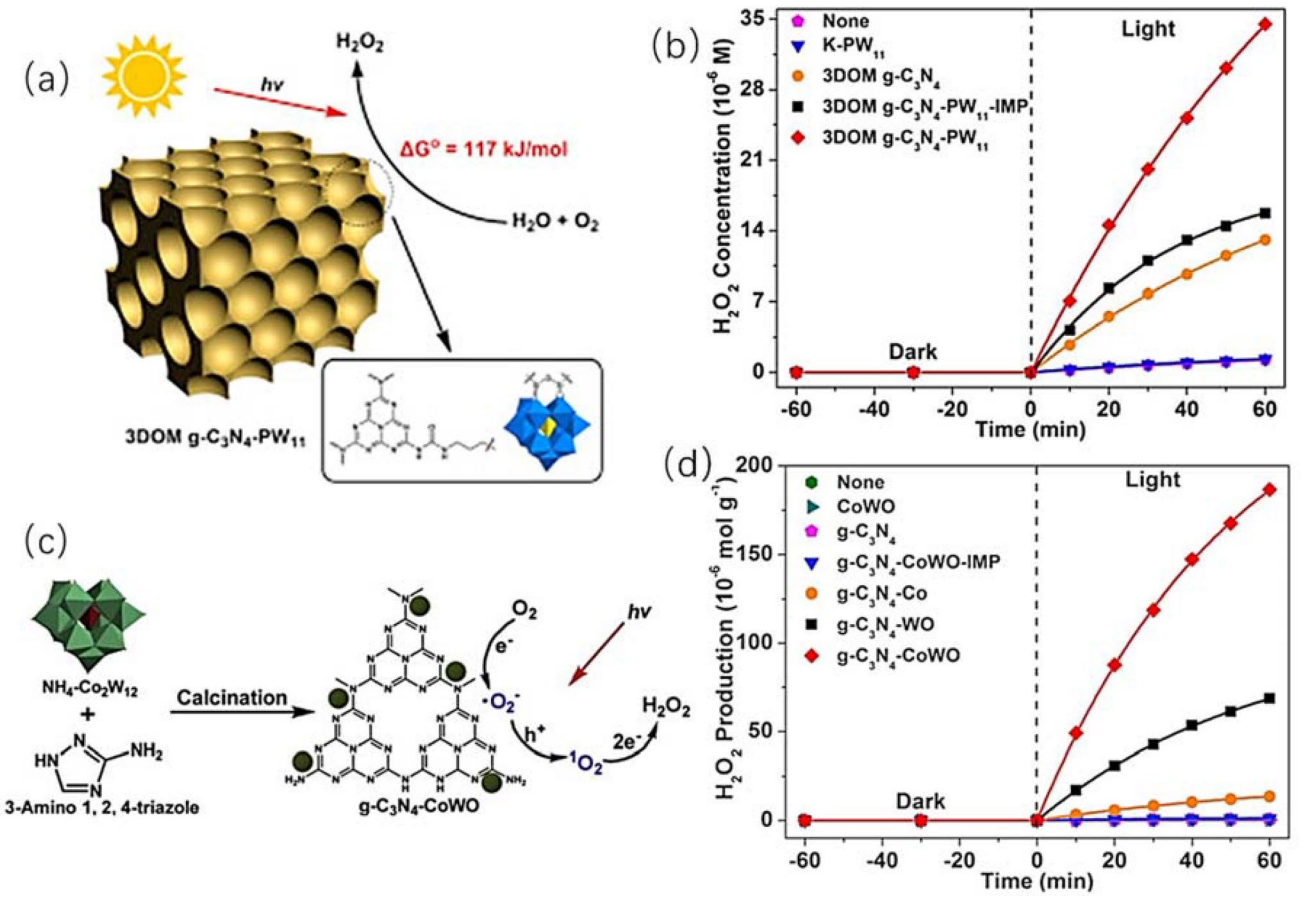

Fig. 8 Photocatalytic H_2O_2 formation pathway over g-C_3N_4-PW_{11} catalyst (**a**) and its H_2O_2 productivity (**b**) [22], copyright 2017 Elsevier; photocatalytic H_2O_2 formation pathway over g-C_3N_4-CoWO (**c**) and its H_2O_2 productivity (**d**) [59], copyright 2019 Elsevier

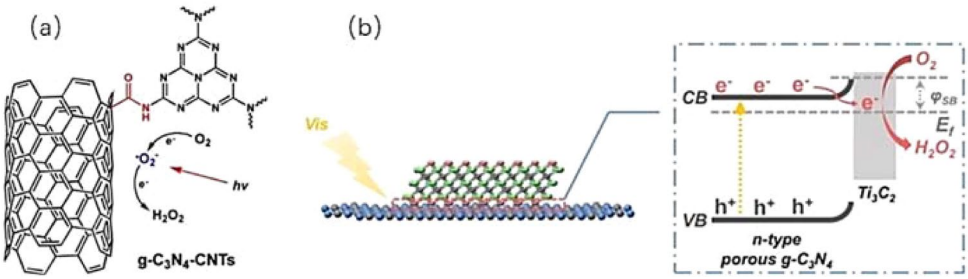

Fig. 9 Schematic diagram of photocatalytic H_2O_2 production over g-C_3N_4-CNTs (**a**) [26], copyright 2018 Elsevier, and TC/pCN (**b**) [62], copyright 2019 Elsevier

The g-C_3N_4 based materials have unique structure of tris-triazine moieties which can promote selective two-electron transfer to O_2 via sequential formation of a superoxo radical and 1,4-endoperoxide species to facilitates H_2O_2 generation under visible light irradiation [63]. The yield and selectivity of H_2O_2 can be enhanced via the improvements in the surface, oxygen affinity, charge separation, proton-coupled electron transfer, and H_2O_2 decomposition retardation of g-C_3N_4 catalysts. Therefore, the strategies of morphology control, hetero-elements doping, surface modification and hybridization for g-C_3N_4 are expected to be further updated and reported. Scaling up of H_2O_2 production can be achieved by the development of g-C_3N_4 materials and their system engineering.

3 Photocatalytic Production of H_2O_2 over TiO_2 Based Materials

TiO_2 based photocatalysts are one of the preferred families for H_2O_2 production due to their merits of chemical stability, low cost and practical application. Before H_2O_2 production

over TiO_2 becomes commercial, it should overcome two difficulties including the side reaction of one electron oxygen reduction, and the serious decomposition of H_2O_2 catalyzed by the intermediate of ≡Ti–OOH. The improved strategies and the categorization for TiO_2 are similar to that for the abovementioned g-C_3N_4 catalysts. The modification strategies, photocatalytic performances and properties of the reported TiO_2 based materials for photocatalytic H_2O_2 production are collected in Table 2.

Single TiO_2 catalyst has obtained the satisfied yield of H_2O_2. Cai et al. earlier researched photocatalytic production of H_2O_2 over TiO_2 [64]. In their work, the effect of copper ions on the formation of H_2O_2 was investigated. In an O_2 purged solution, H_2O_2 productivity was increased to 20 times in the presence of moderate amount of copper ions. Shiraishi's group tried to use benzylic alcohols as hydrogen sources for light driven H_2O_2 production with TiO_2 photocatalyst [30]. They revealed that the enhanced H_2O_2 formation was due to the efficient formation of side-on coordinated per oxo species on the photoactivated TiO_2 surface, via the reaction of benzylic alcohol and O_2. The peroxo species was readily transformed to H_2O_2, thus facilitating highly efficient H_2O_2 production. The band gap photoexcitation of TiO_2 also promoted the selectivity of H_2O_2. In another earlier report, the effect of Zn(II) on the formation of H_2O_2 over TiO_2 was investigated [65]. In this work, the researchers provided the mechanism and kinetic of interfacial electron transfer by blocking surface trapping sites for photogenerated carriers (≡Ti–OH).

There are a number of works on the surface modification strategies for TiO_2 to enhance its H_2O_2 photoproduction. For examples, a Pt/TiO_2 photocatalytic system simultaneously achieved the H_2 and the H_2O_2 production [66]. H_2O_2 productivity reached 5096 μmol g^{-1} h^{-1}, which was attributed to the more favorable two-electron oxidation of water to H_2O_2 than the four-electron oxidation of water to O_2. A negative charged Pd nanoparticles loaded on TiO_2 photocatalyst was prepared by coordinating Pd with surface-anchored organic ligands [67]. The negative charge on the Pd were induced by the electron donation from amine groups of the ligands. For photocatalytic production of H_2O_2, a mechanism was proposed that the electronic tuning of Pd nanoparticles enhanced the charge separation on TiO_2, which improved the selectivity of O_2 reduction to produce H_2O_2. The improved selectivity for H_2O_2 production was over the side reactions such as

Table 2 Summary of the modification strategies, photocatalytic performances and properties of the reported TiO_2 based materials for photocatalytic H_2O_2 production

Photocatalyst	Modification strategy	Reaction system	H_2O_2 productivity	References
TiO_2	Pristine	UV irradiation; 3 mL water, Cu^{2+}; O_2	8 μM (5 min)	[64]
TiO_2	Pristine	Visible light; 5 mL benzyl alcohol/water; O_2	40 mM (12 h)	[30]
Pt/TiO_2	In-situ photo-depostion method	Visible light; 20 mL water	5.1 mmol (1 h)	[66]
Pd/TiO_2	Coordination with surface-anchored organic ligands	Visible light; phosphate buffer	150 μM (1 h)	[67]
Au/porous TiO_2 film	Thermal evaporator	365 nm UV lamp irradiation; Ethanol/Citrate buffer, pH 3.8	1.5 mM (0.5 h)	[68]
SN-GQD/TiO_2	Hydrothermal and impregnation	Visible light; 50 mL water/2-propanol (pH 3)	451 μM (1 h)	[69]
Nf-SNG/TiO_2	Nafion coating	Visible light; 50 mL water/2-propanol (pH = 3)	780 μM (2 h)	[70]
HTNT-CD	Hydrothermal method	Visible light; 30 mL water; O_2	110 μmol (2 h)	[71]
CoPirGO/TiO_2	In-situ formation of cobalt phosphate on photocatalyst	Visible light; 40 mL water/2-propanol; O_2	4.6 mM (3 h)	[31]

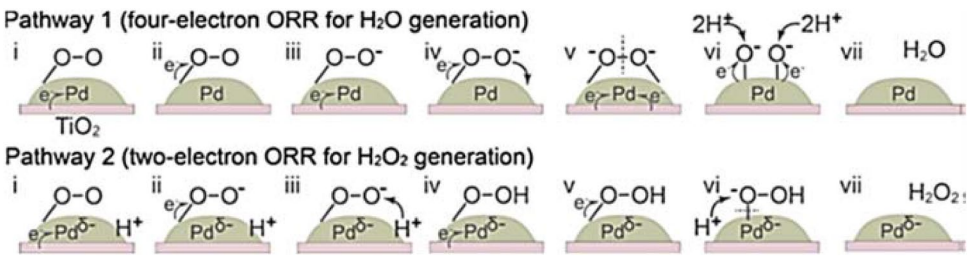

Fig. 10 Mechanisms of oxygen reduction on the surface of Pd nanoparticles [67], copyright 2019 American Chemical Society

O_2 reduction to water (Pathway 1, Fig. 10). O_2 reduction occurred on the Pd surface given the high affinity of O_2 to Pd, generating surface-bound superoxide by the first electron transfer. The selectivity for H_2O_2 production is determined by the subsequent competing coordination reactions: μ-peroxo coordination followed by homolytic O–O bond cleavage (Pathway 1, with water as final product, Fig. 10) vs protonation (Pathway 2, with H_2O_2 as final product, Fig. 10). A porous TiO_2 films supporting Au nano island was exploited as the photocatalyst of light driven H_2O_2 production [68] (Fig. 11a). H_2O_2 concentration over the catalyst achieved the mM scale within 5 min, which was 80-folds based on pure TiO_2 (Fig. 11b). The combination of small Au, TiO_2, and large Au species reduced the potential barriers, and thus reduced the recombination of electron–hole pairs. A CuO incorporated TiO_2 catalyst was earlier prepared for light driven H_2O_2 production [32]. Modification of CuO promoted the charge separation and provided active sites for water reduction. In detail, photoexcited electrons in CB of both TiO_2 and CuO, and the accumulation of excess electrons in CuO caused a negative shift in the Fermi level, which gained the required overvoltage necessary for efficient water reduction reaction. Zheng et al. modified TiO_2 with S and N co-doped graphene quantum dots (SNGQD/TiO_2) for photocatalytic production of H_2O_2 [69]. SNGQD induced the extended visible light absorption and enhanced electron migration. The catalyst exhibited 3.2 times of H_2O_2 yield (451 μmol L^{-1}) as that of bare TiO_2 under simulated sunlight irradiation. The increased H_2O_2 was attributed to the boosted two-electron reduction of oxygen, as well as the suppressed decomposition of H_2O_2. Koutecky–Levich plots and DFT calculations demonstrated that the kinetic rate of ORR was accelerated by GQDs with the facilitated charge transfer, and the two-electron ORR pathway rationalized the high selectivity for H_2O_2 formation. In another work [70], a novel nafion coatings on S,N-codoped graphene-quantum-dots-modified TiO_2 (Nf-SNG/TiO_2) catalyst also presented the enhanced photocatalytic performance of H_2O_2 photoproduction.

Hybridization of carbon materials with TiO_2 based photocatalysts has also been attempted in photocatalytic H_2O_2 production. For examples, a hybrid material of proton-form titania nanotube with carbon dot (HTNT-CD) was exploited for H_2O_2 photoproduction [71]. It was demonstrated that the protons of HTNT-CD were crucial for acceleration of the half reaction of molecular O_2 reduction to form H_2O_2, and hindering the H_2O_2 decomposition. The HTNT-CD hybrid obtained 5.2% of the solar-to-H_2O_2 apparent energy conversion efficiency, which was about 5 times of that over P25 catalyst. In addition, a reduced graphene oxide and TiO_2 (rGO/TiO_2) hybrid system further increased H_2O_2 yield to a mmol scale via the adsorption of phosphate on TiO_2 [31].

TiO_2 based materials have the potential to become mature photocatalysts for visible light-driven H_2O_2 production due to the merits of chemical stability and low cost. However, there are two challenges restricting this application of TiO_2: (1) the dominated inefficient single-electron O_2 reduction; (2) the simultaneous decomposition of H_2O_2 by forming peroxide complexes (≡Ti–OOH) [70]. Therefore, more studies are being concentrated on doping, hybridization or surface decoration for TiO_2 to achieve highly selective two-electron reduction of O_2 and inhibition of photodecomposition of H_2O_2.

4 Photocatalytic Production of H_2O_2 Over Transition Metal Complexes

Metal complexes including the metal–organic frameworks (MOFs) are another family for photocatalytic production of H_2O_2. The modification strategies, photocatalytic performances and properties of the reported transition metal

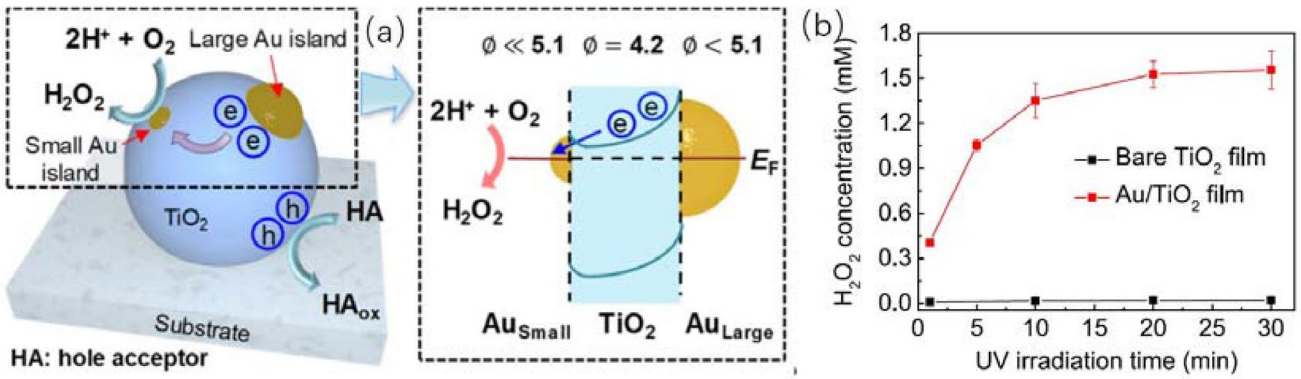

Fig. 11 Schematic diagram of photocatalytic H_2O_2 production over Au/TiO_2 films (**a**) [68], copyright 2019 American Chemical Society; time-dependent H_2O_2 production over bare TiO_2 and Au/TiO_2 films (**b**) [68], copyright 2019 American Chemical Society

Table 3 Summary of the modification strategies, photocatalytic performances and properties of the reported transition metal complexes for photocatalytic H_2O_2 production

Photocatalyst	Modification strategy	Reaction system	H_2O_2 productivity	References
MIL-125-NH_2	Post-synthetic modification with alkyl chains	Visible light; benzylalcohol/water; O_2	2.4 mM (3 h)	[72]
OPA/MIL-125-NH_2	Alkylated process	Visible light; benzylalcohol/water; O_2	6.5 mM (3 h)	[73]
Zn-5-aminoindazole	Pristine	280–360 nm irradiation; water	63 mM/day	[74]
$QuPh^+$–NA	–	334 nm irradiation; acetonitrile–water; O_2	36 mM (5 h)	[46]
$[Ru(Me_2phen)_3]^{2+}$ $Ir(OH)_3$	–	Visible light; water; O_2	612 μM (9 h)	[42]
$[Ru(Me_2phen)_3]^{2+}$ $[Ir(Cp^*)(H_2O)_3]^{2+}$	–	Visible light; water; O_2	2.0 mM (24 h)	[43]
$[Ru(Me_2phen)_3]^{2+}$ $Co_3[Fe(CN)_6]_2$,	–	Visible light; water with Sc^{3+}; O_2	350 μM (15 h)	[40]
Octahedral $Cd_3(C_3N_3S_3)_2$ coordination polymer	Template-free wet-chemical synthesis	Visible light; 20 mL methanol/water, pH 2.8	8.8 mM (4 h)	[36]
xrGO/$Cd_3(TMT)_2$	Stepwise fabrication procedures	Visible light; 20 mL methanol/water; O_2	7.2 mM (25 h)	[37]

complexes for photocatalytic H_2O_2 production are collected in Table 3.

4.1 Metal–Organic Frameworks

Recently, a MIL-125-NH_2 MOFs material for photocatalytic H_2O_2 production in a benzylalcohol/water two-phase system was exploited and reported [72] (Fig. 12a). Hydrophobization of MOF enabled the spontaneous separation of the benzaldehyde formed to the benzylalcohol phase and of the H_2O_2 formed to the aqueous phase (Fig. 12b). The novel system enhanced the photocatalytic efficiency and adapted various mediums including a solution of low pH for H_2O_2 production. Meanwhile, the same group modified MIL-125-NH_2 MOFs via alkylation of octadecylphosphonic acid (OPA/MIL-125-NH_2) as a photocatalyst for H_2O_2 production [73] (Fig. 12c). The enhanced photocatalytic performance originated from Ti cluster-alkylated hydrophobic property, and the faster diffusion of reactants and products in the maintained pores of the MOFs.

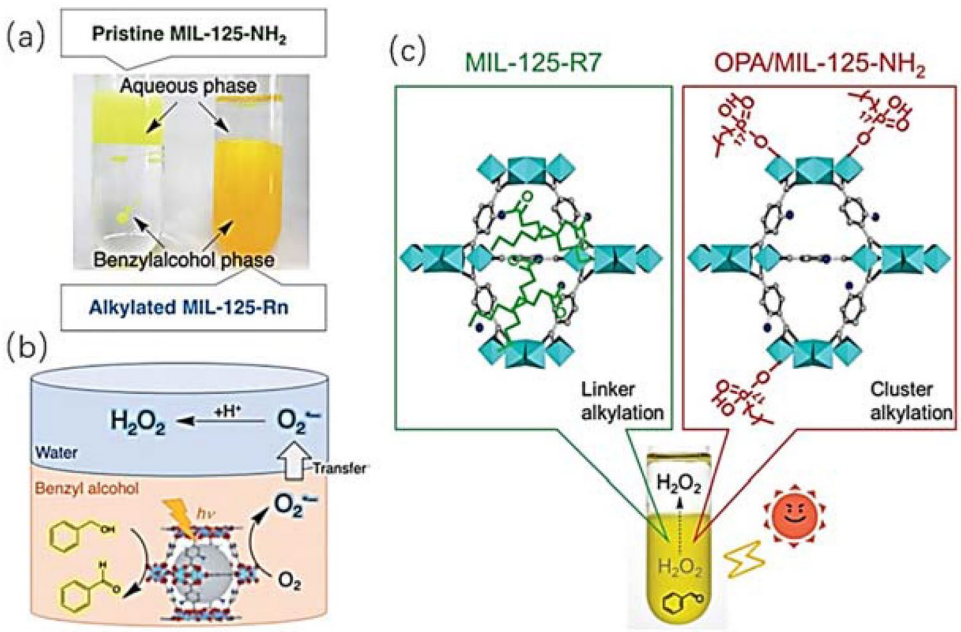

Fig. 12 Photographs of two-phase systems composed of an aqueous phase and a benzylalcohol phase containing MIL-125-NH_2 (left) and MIL-125-Rn (right) (**a**); photocatalytic H_2O_2 production utilizing the two-phase system (**b**) [72], copyright 2019 Wiley; structures of linker-alkylated MIL-125-NH_2, MIL-125-R7 (top left), cluster-alkylated MIL-125-NH_2, OPA/MIL-125-NH_2 (top right), and photocatalytic H_2O_2 production over the MOFs system [73], copyright 2019 Royal Society of Chemistry

4.2 Novel Transition Metal Complexes

In 2005, Hayes et al. earlier reported Zn(II)-centered complexes acting as photocatalysts for H_2O_2 production in an ultraviolet irradiated environment [74]. In this work, various ligands of amino-substituted isomers including indazole, pyridine, and phenylenediamine et al. were tested to catalyze the reaction. Among them, Zn-5-aminoindazole obtained the greatest first-day production of 63 mM/day with a 37% quantum yield and *p*-phenylenediamine (PPAM) showed the greatest long-term stability.

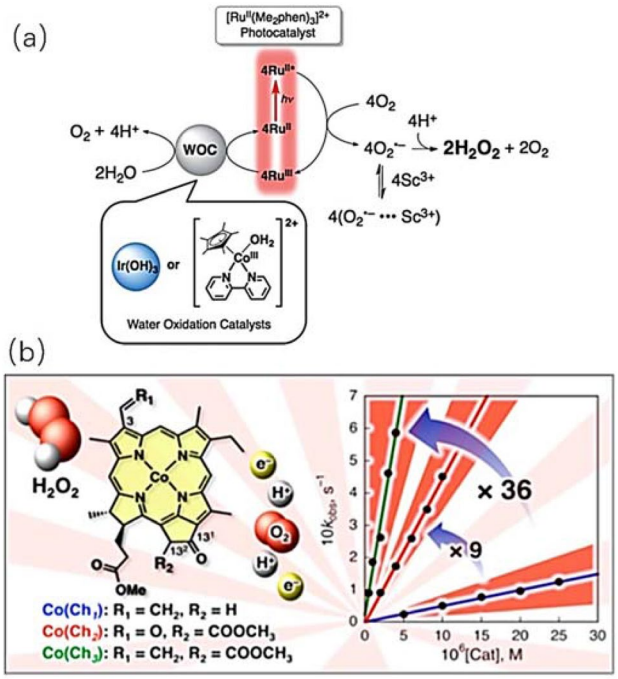

Fig. 13 Schematic diagram of photocatalytic H_2O_2 production over $[Ru^{II}(Me_2phen)_3]^{2+}$-$Ir(OH)_3$-$Sc^{3+}$ system (**a**) [42], copyright 2013 Royal Society of Chemistry, and ($Co^{II}(Ch_n)$ system (**b**) [44], copyright 2015 American Chemical Society

After that, most of the reports on applying the transition metal complexes in photocatalytic H_2O_2 production were from Fukuzumi's group. For examples, they reported photocatalytic H_2O_2 production over a complex catalyst of 2-phenyl-4-(1-naphthyl)quinolinium ion ($QuPh^+$–NA) with oxalate or oxalic acid as electron donor [45, 46]. $QuPh^+$–NA formed the long-lived electron-transfer state upon the photoexcitation with strong oxidation ability. In an oxygen saturated mixed solution of a buffer and acetonitrile, 14% of quantum yield and 93% of H_2O_2 yield were obtained. $[Ru(Me_2phen)_3]^{2+}$ (Me_2phen = 4,7-dimethyl-1,10-phenanthroline) and $Ir(OH)_3$ was used as photocatalysts for water oxidation in an O_2-saturated H_2SO_4 aqueous solution [42]. H_2O_2 was produced from the formation of $[Ru^{III}(Me_2phen)_3]^{3+}$ and $\cdot O^{2-}$, which resulted from the electron transfer from the excited state of $[Ru^{II}(Me_2phen)_3]^{2+}$ to O_2. Photocatalytic activity was further improved by replacing $Ir(OH)_3$ nanoparticles by $[Co^{III}(Cp^*)(bpy)(H_2O)]^{2+}$ in the presence of $Sc(NO_3)_3$ in water (Fig. 13a). After that, they employed nanoparticles composed of earth abundant nickel and iron ($NiFe_2O_4$) instead of the Ir complex as a water oxidation catalyst for the photocatalytic production of H_2O_2 [43]. During the reaction, $NiFe_2O_4$ nanoparticles were formed from the corresponding as-prepared $NiFe_2O_4$. The H_2O_2 productivity also achieved improvement. They also used cyano-bridged a polynuclear complexes $(Fe_xCo_{1-x})_3$ $[Co(CN)_6]_2$ as effective catalysts for photocatalytic H_2O_2 production in an O_2-saturated aqueous solution in the presence of $[Ru(Me_2phen)_3]^{2+}$ and $Sc(NO_3)_3$ under visible light irradiation [40]. Cobalt chlorin derivatives ($Co^{II}(Ch_n)$ (n = 1–3)) was used as catalyst for investigation on the mechanism of photocatalytic H_2O_2 production [44]. Nonsubstituted cobalt chlorin complex ($Co^{II}(Ch_1)$) efficiently and selectively catalyzed two-electron reduction of O_2 by a one-electron reductant (1,1′-dimethylferrocene) to produce H_2O_2 in the presence of perchloric acid ($HClO_4$) in benzonitrile (Fig. 13b). The change in redox property resulted in the enhancement of the catalytic reactivity, where the observed rate constant (k_{obs})

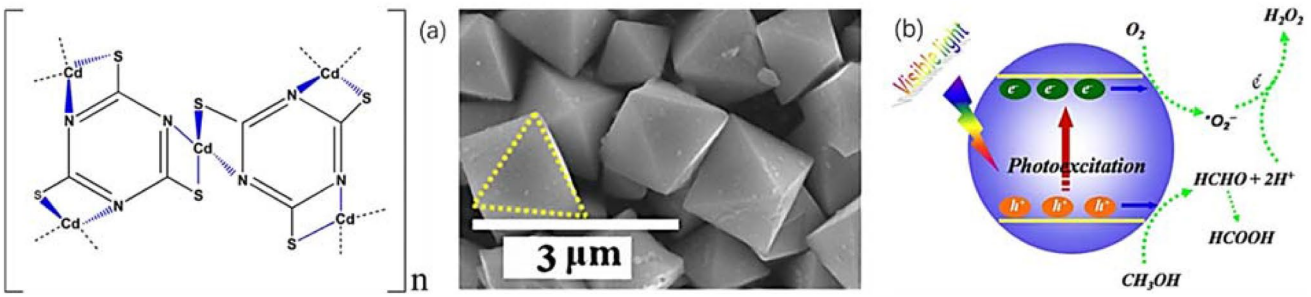

Fig. 14 Structure and SEM image of $Cd_3(C_3N_3S_3)_2$ coordination polymer (**a**), and its photocatalytic H_2O_2 production pathway (**b**) [36], copyright 2015 Nature

value of $Co^{II}(Ch_3)$ was 36-fold larger than that of $Co^{II}(Ch_1)$ (Fig. 13b).

In addition to the above work, an octahedral $Cd_3(C_3N_3S_3)_2$ coordination polymer was exploited and enhanced photocatalytic H_2O_2 production from methanol/water solution [36] (Fig. 14a, b). Later, the octahedron $Cd_3(C_3N_3S_3)_2$ was adhered to the reduced graphene (rGO) (xrGO/$Cd_3(TMT)_2$) to become a improved photocatalyst for visible light-driven H_2O_2 production [37]. The formation of H_2O_2 was 2.5-folds enhanced and its deformation was concurrently suppressed. The enhanced performance mainly resulted from the accelerated charge transfer process, which was originated from the supreme electrically conductive properties of graphene.

Transition metal complexes including MOFs materials possess the attractive features that their structures can be modified and regulated from 2 to 3D to achieve desired properties. The transition metal complexes as novel photocatalysts for visible light-driven H_2O_2 production can provide appropriate bandgaps and one-electron components to efficiently and selectively promote the two-electron reduction of O_2 after modification. The unique systems of transition metal complexes are worthy of in-depth studying.

5 Other Semiconductor Materials

The modification strategies, photocatalytic performances and properties of other semiconductor materials for photocatalytic H_2O_2 production are collected in Table 4.

5.1 ZnO Based Materials

ZnO is a type of semiconductor to be earlier reported in the field of photocatalytic H_2O_2 production. In 1988, Hoffmann's group used ZnO contained illuminated aqueous suspension for photocatalytic H_2O_2 production in the presence of O_2 and organic electron donors [28]. They proposed that H_2O_2 could be produced through reduction of O_2 by CB electrons, and the yield of photogenerated CB electrons could be increased by adding electron donors. Later, they used aqueous suspensions of transparent quantum-sized ZnO semiconductor colloids to produce steady-state concentrations of H_2O_2 as high as 2 mM [75]. The initial rate of H_2O_2 production was 100–1000 times faster with quantum-sized ZnO than that with bulky ZnO.

5.2 Transition Metal Sulfide-Based Materials

CdS is employed to be an efficient catalyst since its relatively high CB edge position is advantageous for O_2 reduction and the subsequent H_2O_2 production. Kim et al. started with silica nanocapsules (SNCs) that host CdS photocatalysts on their shell surfaces to achieve photocatalytic production of H_2O_2 through sensitized triplet–triplet annihilation (TTA) upconversion (UC) of low-energy, sub-bandgap photons. They further loaded a graphene oxide nanodisk (GOND) as a co-catalyst (GOND/CdS–SNC) [35]. The photogenerated electrons were efficiently transferred into GOND to retard rapid charge recombination in CdS, which subsequently reduced dioxygen to produce H_2O_2 up to a 100 mmol level per hour. Later, a CdS-reduced graphene oxide (RGO) hybrid achieved photocatalytic production of H_2O_2 under sunlight from water and O_2 without using organic electron donors [34]. The optimal catalyst showed five times of H_2O_2 production higher than CdS nanoparticles. Photocatalytic reaction was mainly proceeded by two-electron reduction of O_2 rather than water oxidation on the catalyst surface. The CB level of CdS was demonstrated to be more negative than the reduction potential of O_2, which was sufficient for the high selectivity for the two-electron reduction of O_2 (Fig. 15). In addition, the photocatalytic system was suitable to be operated at lower temperature and pH.

In a recent work of our group, atomic-scale Au modified MoS_2 nanosheets as a photocatalyst for light driven H_2O_2 production was prepared via a simple pathway including the deposition-reduction and immobilization process [38]. Au modification brought out the low recombination rate of e^-–h^+ pairs, long lifetime of electrons and more negative flat band potential for MoS_2. The catalyst achieved efficient photocatalytic production of H_2O_2 from H_2O and air in the

Table 4 Summary of the modification strategies, photocatalytic performances and properties of other materials for photocatalytic H_2O_2 production

Photocatalyst	Modification strategy	Reaction system	H_2O_2 productivity	References
GOND/CdS–SNC	Emulsification, sol–gel, exfoliation	Visible light; alcohol/water; O_2	92 μM (1 h)	[35]
CdS-RGO	Hydrothermal method	Sunlight; 50 mL water contained H_2SO_4; O_2	128 μM (12 h)	[34]
Atomic Au@MoS_2	Reduction, deposition	Sunlight; 50 mL water, pH 9	792 μM (6 h)	[38]
Au/$BiVO_4$	Deposition precipitation	Visible light; 30 mL EtOH/water; O_2	40 μM (10 h)	[39]
Polymer supported carbon dots	Hydrothermal, mechanical, ultrasonic	Visible light; EtOH/water; O_2	83 μM (50 h)	[77]
Graphene oxide	Pristine	Visible light; 7 mL of GO suspension; O_2	195 μM (6 h)	[19]

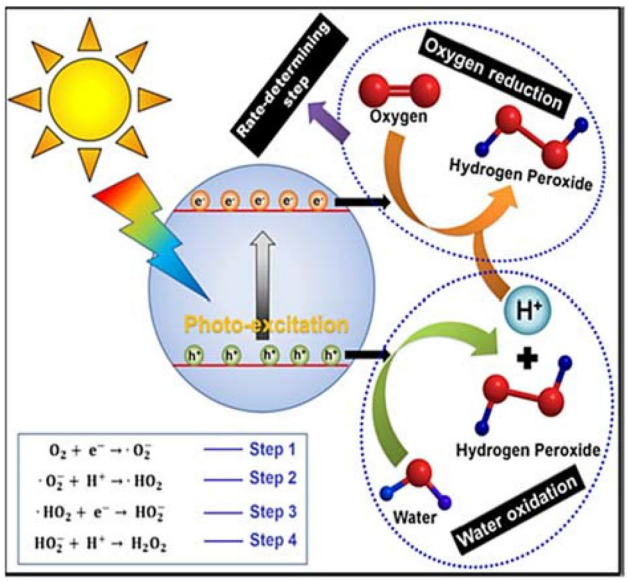

Fig. 15 Plausible mechanism for production of H_2O_2 by CdS-G hybrid under sunlight [34], copyright 2017 Elsevier

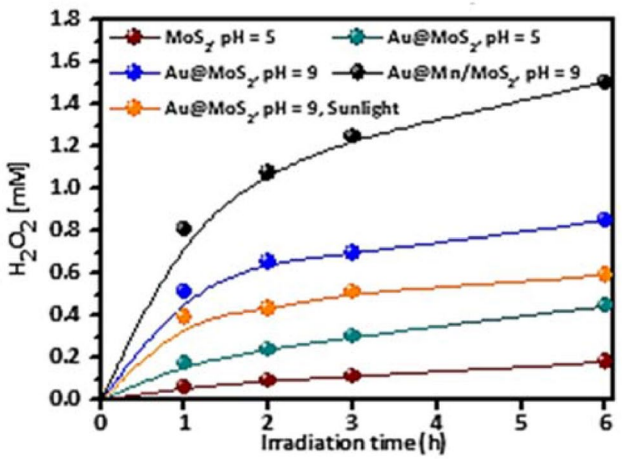

Fig. 16 Photocatalytic H_2O_2 production over atomic-scale Au modified MoS_2 nanosheets under different conditions [38] copyright 2019 Elsevier

absence of pure O_2 and organic electron donors. An optimal catalyst enhanced the H_2O_2 productivity by about 2.5 times based on bare MoS_2. The H_2O_2 productivity at pH 9 was further enhanced by 7.4 times based on that at pH 2 (Fig. 16).

In recent years, the application potential of transition metal sulfides gradually emerges in the field of photocatalytic H_2O_2 production. The VB tops of some transition metal sulfides locate at an appropriate range, which provide the strong thermodynamic driving force for water oxidation. In addition, the CB levels of some transition metal sulfides are more negative than the reduction potential of O_2, which provide enough potential for O_2 reduction. Therefore, it is advised that more sorts of transition metal sulfides can be explored in photocatalytic H_2O_2 production systems.

5.3 Bi Containing Semiconductors

$BiVO_4$ loaded with Au nanoparticles was first reported for photocatalytic production of H_2O_2 in pure water with O_2 [39]. The bottom of the $BiVO_4$ conduction band was more positive than the one-electron reduction potential of O_2 while more negative than the two-electron reduction potential of O_2 (Fig. 17). Therefore, one-electron reduction of O_2 was suppressed and the selectivity for two-electron reduction of O_2 was promoted, resulting in efficient H_2O_2 formation. In a Later work, plasmonic $Bi/Bi_2O_{2-x}CO_3$ with surface oxygen vacancies was synthesized for photocatalytic production of H_2O_2, and the role of in situ generated H_2O_2 for photocatalytic removal of gaseous NO_x was investigated [76]. In-situ introduction of plasmonic Bi on the surface of $Bi_2O_{2-x}CO_3$ promoted the generation of H_2O_2 at mM scale by capturing electrons from the defect states of $Bi_2O_{2-x}CO_3$ via the two-electron reduction of O_2. The dissociation of H_2O_2 was concluded to be interdicted by the in situ formation of Bi, which suppressed the single electron reduction of H_2O_2 to ·OH and enhanced the selectivity of O_2 reduction to H_2O_2. The presence of oxygen vacancies in $Bi/Bi_2O_{2-x}CO_3$ was critical to H_2O_2 production selectivity. The above two works presented the feasibility of photocatalytic production of H_2O_2 over the Bi containing semiconductors.

5.4 Carbon Materials

Carbon family including graphene nanomaterials are emerging photocatalysts consisting of earth-abundant elements. A carbon dot-impregnated waterborne hyperbranched polyurethane was developed as a heterogeneous photocatalyst for solar driven production of H_2O_2 in the presence of C_2H_5OH and O_2 [77]. The carbon dots possessed a suitable bandgap of 2.98 eV, which facilitated effective splitting of both water and ethanol under solar irradiation. In the system, photoreaction of C_2H_5OH with H_2O around room temperature promoted selective H_2O_2 production. In another report,

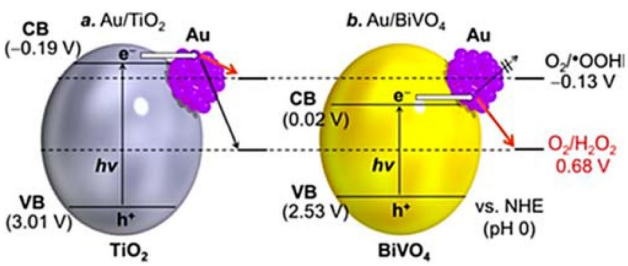

Fig. 17 Energy diagrams for Au/TiO_2 and $Au/BiVO_4$ and reduction potential of O_2 [39] copyright 2016 American Chemical Society

graphene oxide could efficiently catalyzed photogeneration of H_2O_2 to mmol levels in the absence of electron donors [19]. It was found that the dissolved O_2 contributed to the H_2O_2 generation, and H_2O_2 photoproduction was readily enhanced by raising pH.

6 Summary and Outlook

Nowadays, photocatalytic production of H_2O_2 is becoming a research hotspot, because it exhibits cost-efficient and eco-friendly advantages, and can adapt to the applications of environmental remediation, organic synthesis and fuel cells. This minireview covers most of the advanced catalysts and techniques of H_2O_2 photoproduction, and highlights the advanced modification strategies for semiconductor catalysts to enhance their H_2O_2 productivity. So far, various photocatalyst families have been explored, such as ZnO, g-C_3N_4, TiO_2, metal complexes, metal sulfides, Bi containing semiconductors, and carbon materials et al. Modification strategies are mainly classified as structure/morphology modulation, surface decoration, elements doping, and semiconductors hybridization. The modifications mainly aim at increase in the inner space of semiconductors, activation of the molecular O_2, inhibition of the photocarriers recombination, promotion of the electron transfer, and weakening the photocatalytic H_2O_2 decomposition. Photocatalytic H_2O_2 production technique is developing in a challenging stage, and thus it has huge space to become mature. The technique still faces the issues that the H_2O_2 productivity is expected to be increased into a higher scale, the use of electron donors and pure O_2 should be lowered, the selectivity of two-electron reduction of O_2 requires to be further increased over one- or four-electron reduction of O_2. The fundamental solution of all the issues is to explore more efficient semiconductor catalysts, as well as their synthesis and modification strategies. The key avenues should focus on modulating the electron structure of semiconductors, suppressing the decomposition of as-prepared H_2O_2, and enhancing the activation and utilization of O_2. Moreover, the mechanisms of various photocatalytic H_2O_2 production systems are also necessary to be investigated in depth to design and optimize the photocatalysts with high efficiency. In this regard, researchers may employ high-efficiency characterization methods to study the morphology and photoelectric properties of photocatalysts, and use theory calculation approaches to design and study the photocatalytic H_2O_2 production system. We expect that the photocatalytic H_2O_2 production is now in progress along with more and more novel synthetic strategies of photocatalyst and improved procedures.

Acknowledgements This project was supported by Heilongjiang Provincial Natural Science Foundation of China (Grant No. LH2019B023), the China Postdoctoral Science Foundation funded project (Grant No. 2016M601403), and the Scientific Research Project of Harbin Institute of Petroleum (Grant No. HIPJJ201917).

References

1. Sato K, Aoki M, Noyori R (1998) A "Green" route to adipic acid: direct oxidation of cyclohexenes with 30 percent hydrogen peroxide. Science 281:1646–1647
2. Niwa S-i, Eswaramoorthy M, Nair J, Raj A, Itoh N, Shoji H, Namba T, Mizukami F (2002) A one-step conversion of benzene to phenol with a palladium membrane. Science 295:105–107
3. Shaegh SAM, Nguyen N-T, Ehteshamiab SMM, Chan SH (2012) A membraneless hydrogen peroxide fuel cell using Prussian Blue as cathode material. Energy Environ Sci 5:8225–8228
4. Fukuzumi S (2017) Production of liquid solar fuels and their use in fuel cells. Joule 1:689–738
5. Fukuzumi S (2016) Artificial photosynthesis for production of hydrogen peroxide and its fuel cells. Biochim Biophys Acta 1857:604–611
6. Campos-Martin JM, Blanco-Brieva G, Fierro JLG (2006) Hydrogen peroxide synthesis: an outlook beyond the anthraquinone process. Angew Chem Int Ed 45:6962–6984
7. Hou H, Zeng X, Zhang X (2019) Production of hydrogen peroxide through photocatalytic processes: a critical review of recent advances. Angew Chem Int Ed. https://doi.org/10.1002/anie.201911609
8. Sheldon RA, Arends IWCE (2004) Organocatalytic oxidations mediated by nitroxyl radicals. Adv Synth Catal 346:1051–1071
9. Foller PC, Bombard RT (1995) Processes for the production of mixtures of caustic soda and hydrogen peroxide via the reduction of oxygen. J Appl Electrochem 25:613–627
10. Edwards JK, Solsona BE, Landon P, Carley AF, Herzing A, Kiely CJ, Hutchings GJ (2005) Direct synthesis of hydrogen peroxide from H_2 and O_2 using TiO_2-supported Au–Pd catalysts. J Catal 236:69–79
11. Song H, Li G, Wang X, Chen Y (2011) Characterization and catalytic performance of Au/Ti-HMS for direct generation of H_2O_2 and in situ-H_2O_2-ODS from H_2 and O_2: an in situ-reduction synthesis and a recycle study of catalyst. Microporous Mesoporous Mat 139:104–109
12. Edwards JK, Solsona B, Carley AF, Herzing AA, Kiely CJ, Hutchings GJ (2009) Switching off hydrogen peroxide hydrogenation in the direct synthesis process. Science 323:1037–1041
13. Edwards JK, Pritchard J, Piccinini M, Shaw G, He Q, Carley AF, Kiely CJ, Hutchings GJ (2012) The effect of heat treatment on the performance and structure of carbon-supported Au–Pd catalysts for the direct synthesis of hydrogen peroxide. J Catal 292:227–238
14. Henkel H, Weber W (Henkel & CIE) (1914) US1108752 [Chem. Abstr. 1914, 8, 23927].
15. Li S, Dong G, Hailili R, Yang L, Li Y, Wang F, Zeng Y, Wang C (2016) Effective photocatalytic H_2O_2 production under visible light irradiation at g-C_3N_4 modulated by carbon vacancies. Appl Catal B 190:26–35
16. Baur E, Neuweiler C (1927) Photolytic formation of hydrogen-peroxide. Helv. Chim Acta 10:901–907
17. Yang L, Dong G, Jacobs DL, Wang Y, Zang L, Wang C (2017) Two-channel photocatalytic production of H_2O_2 over g-C_3N_4 nanosheets modified with perylene imides. J Catal 352:274–281
18. Zhu Z, Pan H, Murugananthan M, Gong J, Zhang Y (2018) Visible light-driven photocatalytically active g-C_3N_4 material for enhanced generation of H_2O_2. Appl Catal B 232:19–25

19. Hou W-C, Wang Y-S (2017) Photocatalytic generation of H_2O_2 by graphene oxide in organic electron donor-free condition under sunlight. ACS Sustain Chem Eng 5:2994–3001
20. Shiraishi Y, Kanazawa S, Sugano Y, Tsukamoto D, Sakamoto H, Ichikawa S, Hirai T (2014) Highly selective production of hydrogen peroxide on graphitic carbon nitride (g-C_3N_4) photocatalyst activated by visible light. ACS Catal 4:774–780
21. Shiraishi Y, Kanazawa S, Kofuji Y, Sakamoto H, Ichikawa S, Tanaka S, Hirai T (2014) Sunlight-driven hydrogen peroxide production from water and molecular oxygen by metal-free photocatalysts. Angew Chem Int Ed 53:13454–13459
22. Zhao S, Zhao X, Zhang H, Li J, Zhu Y (2017) Covalent combination of polyoxometalate and graphitic carbon nitride for light-driven hydrogen peroxide production. Nano Energy 35:405–414
23. Hu S, Qu X, Li P, Wang F, Li Q, Song L, Zhao Y, Kang X (2018) Photocatalytic oxygen reduction to hydrogen peroxide over copper doped graphitic carbon nitride hollow microsphere: the effect of Cu(I)-N active sites. Chem Eng J 334:410–418
24. Kofuji Y, Ohkita S, Shiraishi Y, Sakamoto H, Tanaka S, Ichikawa S, Hirai T (2016) Graphitic carbon nitride doped with biphenyl diimide: efficient photocatalyst for hydrogen peroxide production from water and molecular oxygen by sunlight. ACS Catal 6:7021–7029
25. Shiraishi Y, Kofuji Y, Sakamoto H, Tanaka S, Ichikawa S, Hirai T (2015) Effects of surface defects on photocatalytic H_2O_2 production by mesoporous graphitic carbon nitride under visible light irradiation. ACS Catal 5:3058–3066
26. Zhao S, Guo T, Li X, Xue T, Yang B, Zhao X (2018) Carbon nanotubes covalent combined with graphitic carbon nitride for photocatalytic hydrogen peroxide production under visible light. Appl Catal B 224:725–732
27. Kim S, Moon G-h, Kim H, Mun Y, Zhang P, Lee J, Choi W (2018) Selective charge transfer to dioxygen on KPF6-modified carbon nitride for photocatalytic synthesis of H_2O_2 under visible light. J Catal 357:51–58
28. Kormann C, Bahnemann DW, Hoffmann MR (1988) Photocatalytic production of H_2O_2 and organic peroxides in aqueous suspensions of TiO_2, ZnO, and desert sand. Envlron Sci Technol 22:798–806
29. Tsukamoto D, Shiro A, Shiraishi Y, Sugano Y, Ichikawa S, Tanaka S, Hirai T (2012) Photocatalytic H_2O_2 production from ethanol/O_2 system using TiO_2 loaded with Au–Ag bimetallic alloy nanoparticles. ACS Catal 2:599–603
30. Shiraishi Y, Kanazawa S, Tsukamoto D, Shiro A, Sugano Y, Hirai T (2013) Selective hydrogen peroxide formation by titanium dioxide photocatalysis with benzylic alcohols and molecular oxygen in water. ACS Catal 3:2222–2227
31. Moon G-h, Kim W, Bokare AD, Sung N-e, Choi W (2014) Solar production of H_2O_2 on reduced graphene oxide-TiO_2 hybrid photocatalysts consisting of earth-abundant elements only. Energy Environ Sci 7:4023–4028
32. Bandara J, Udawatta CPK, Rajapakse CSK (2005) Highly stable CuO incorporated TiO_2 catalyst for photocatalytic hydrogen production from H_2O. Photochem Photobiol Sci 4:857–861
33. Maurino V, Minero C, Mariella G, Pelizzetti E (2005) Sustained production of H_2O_2 on irradiated TiO_2-fluoride systems. Chem Commun 20:2627–2629
34. Thakur S, Kshetri T, Kim NH, Lee JH (2017) Sunlight-driven sustainable production of hydrogen peroxide using a CdS-graphene hybrid photocatalyst. J Catal 345:78–86
35. Kim H-I, Kwon OS, Kim S, Choi W, Kim J-H (2016) Harnessing low energy photons (635 nm) for the production of H_2O_2 using upconversion nanohybrid photocatalysts. Energy Environ Sci 9:1063–1073
36. Zhuang H, Yang L, Xu J, Li F, Zhang Z, Lin H, Long J, Wang X (2015) Robust photocatalytic H_2O_2 production by octahedral $Cd_3(C_3N_3S_3)_2$ coordination polymer under visible light. Sci Rep 5:16947
37. Xu J, Chen Z, Zhang H, Lin G, Lin H, Wang X, Long J (2017) $Cd_3(C_3N_3S_3)_2$ coordination polymer/graphene nanoarchitectures for enhanced photocatalytic H_2O_2 production under visible light. Sci Bull 62:610–618
38. Song H, Wei L, Chen C, Wen C, Han F (2019) Photocatalytic production of H_2O_2 and its in situ utilization over atomic-scale Au modified MoS_2 nanosheets. J Catal 376:198–208
39. Hirakawa H, Shiota S, Shiraishi Y, Sakamoto H, Ichikawa S, Hirai T (2016) Au nanoparticles supported on $BiVO_4$: effective inorganic photocatalysts for H_2O_2 production from water and O_2 under visible light. ACS Catal 6:4976–4982
40. Isaka Y, Oyama K, Yamada Y, Suenobu T, Fukuzumi S (2016) Photocatalytic production of hydrogen peroxide from water and dioxygen using cyano-bridged polynuclear transition metal complexes as water oxidation catalysts. Catal Sci Technol 6:681–684
41. Mase K, Yoneda M, Yamada Y, Fukuzumi S (2016) Efficient photocatalytic production of hydrogen peroxide from water and dioxygen with bismuth vanadate and a cobalt(II) chlorin complex. ACS Energy Lett 1:913–919
42. Kato S, Jung J, Suenobua T, Fukuzumi S (2013) Production of hydrogen peroxide as a sustainable solar fuel from water and dioxygen. Energy Environ Sci 6:3756–3764
43. Isaka Y, Kato S, Hong D, Suenobu T, Yamada Y, Fukuzumi S (2015) Bottom-up and top-down methods to improve catalytic reactivity for photocatalytic production of hydrogen peroxide using a Ru-complex and water oxidation catalysts. J Mater Chem A 3:12404–12412
44. Mase K, Ohkubo K, Fukuzumi S (2015) Much enhanced catalytic reactivity of cobalt chlorin derivatives on two-electron reduction of dioxygen to produce hydrogen peroxide. Inorg Chem 54:1808–1815
45. Yamada Y, Nomura A, Miyahigashia T, Fukuzumi S (2012) Photocatalytic production of hydrogen peroxide by two-electron reduction of dioxygen with carbon-neutral oxalate using a 2-phenyl-4-(1-naphthyl)quinolinium ion as a robust photocatalyst. Chem Commun 48:8329–8331
46. Yamada Y, Nomura A, Miyahigashi T, Ohkubo K, Fukuzumi S (2013) Acetate induced enhancement of photocatalytic hydrogen peroxide production from oxalic acid and dioxygen. J Phys Chem A 117:3751–3760
47. Shiraishi Y, Kanazawa S, Kofuji Y, Sakamoto H, Ichikawa S, Tanaka S, Hirai T (2014) Sunlight-driven hydrogen peroxide production from water and molecular oxygen by metal-free photocatalysts. Angew Chem Int Ed 53:1–7
48. Ou H, Yang P, Lin L, Anpo M, Wang X (2017) Carbon nitride aerogels for the photoredox conversion of water. Angew Chem Int Ed 56:10905–10910
49. Li S, Dong G, Hailili R, Yang L, Li Y, Wang F, Zeng Y, Wang C (2016) Effective photocatalytic H_2O_2 production under visible lightirradiation at g-C_3N_4 modulated by carbon vacancies. Appl Catal B 190:26–35
50. Lu N, Liu N, Hui Y, Shang K, Jiang N, Li J, Yan W (2020) Characterization of highly effective plasma-treated g-C_3N_4 and application to the photocatalytic H_2O_2 production. Chemosphere 241:124927
51. Moon G-h, Fujitsuka M, Kim S, Majima T, Wang X, Choi W (2017) Eco-friendly photochemical production of H_2O_2 through O_2 reduction over carbon nitride frameworks incorporated with multiple heteroelements. ACS Catal 7:2886–2895
52. Tian J, Wu T, Wang D, Pei Y, Qiao M, Zong B (2019) One-pot synthesis of potassium and phosphorus-doped carbon nitride catalyst derived from urea for highly efficient visible light-driven hydrogen peroxide production. Catal Today 330:171–178

53. Xue F, Si Y, Wang M, Liu M, Guo L (2019) Toward efficient photocatalytic pure water splitting for simultaneous H_2 and H_2O_2 production. Nano Energy 62:823–831
54. Teranishi M, Naya S-i, Tada H (2010) In situ liquid phase synthesis of hydrogen peroxide from molecular oxygen using gold nanoparticle-loaded titanium(IV) dioxide photocatalyst. J Am Chem Soc 132:7850–7851
55. Zuo G, Liu S, Wang L, Song H, Zong P, Hou W, Li B, Guo Z, Meng X, Du Y, Wang T, Roye VAL (2019) Finely dispersed Au nanoparticles on graphitic carbon nitride as highly active photocatalyst for hydrogen peroxide production. Catal Commun 123:69–72
56. Yang Y, Zhang C, Huang D, Zeng G, Huang J, Lai C, Zhou C, Wang W, Guo H, Xue W, Deng R, Cheng M, Xiong W (2019) Boron nitride quantum dots decorated ultrathin porous g-C_3N_4: intensified exciton dissociation and charge transfer for promoting visible-light-driven molecular oxygen activation. Appl Catal B 245:87–99
57. Li H, Pang S, Feng X, Müllen K, Bubeck C (2010) Polyoxometalate assisted photoreduction of graphene oxide and its nanocomposite formatio. Chem Commun 46:6243–6245
58. Ma H, Li C, Yin J, Pu X, Zhang D, Su C, Wang X, Shao X (2016) Polyoxometalate enhances the photocatalytic performance of polyaniline/SnO_2 composites. Mater Lett 168:103–106
59. Zhao S, Zhao X (2019) Insights into the role of singlet oxygen in the photocatalytic hydrogen peroxide production over polyoxometalates-derived metal oxides incorporated into graphitic carbon nitride framework. Appl Catal B 250:408–418
60. Fu Y, Ca L, Zhang M, Zhu C, Li H, Wang H, Song Y, Huang H, Liu Y, Kang Z (2018) Photocatalytic H_2O_2 and H_2 generation from living chlorella vulgaris and carbon micro particle comodified g-C_3N_4. Adv Energy Mater 8:1802525
61. Wang X, Han Z, Yu L, Liu C, Liu Y, Wu G (2018) Synthesis of full-spectrum-response $Cu_2(OH)PO_4$/g-C_3N_4 photocatalyst with outstanding photocatalytic H_2O_2 production performance via a "two channel route". ACS Sustain Chem Eng 6:14542–14553
62. Yang Y, Zeng Z, Zeng G, Huang D, Xiao R, Zhang C, Zhou C, Xiong W, Wang W, Cheng M, Xue W, Guo H, Tang X, He D (2019) Ti_3C_2 Mxene/porous g-C_3N_4 interfacial Schottky junction for boosting spatial charge separation in photocatalytic H_2O_2 production. Appl Catal B 258:117956
63. Haider Z, Cho H-I, Moon G-H, Kim H-I (2019) Minireview: Selective production of hydrogen peroxide as a clean oxidant over structurally tailored carbon nitride photocatalysts. Catal Today 335:55–64
64. Cai R, Kubota Y, Fujishima A (2003) Effect of copper ions on the formation of hydrogen peroxide from photocatalytic titanium dioxide particles. J Catal 219:214–218
65. Maurino V, Minero C, Pelizzetti E, Mariella G, Arbezzano A, Rubertelli F (2007) Influence of Zn(II) adsorption on the photocatalytic activity and the production of H_2O_2 over irradiated TiO_2. Res Chem Intermed 33:319–332
66. Wang L, Cao S, Guo K, Wu Z, Ma Z, Piao L (2019) Simultaneous hydrogen and peroxide production by photocatalytic water splitting. Chin J Catal 40:470–475
67. Chu C, Huang D, Zhu Q, Stavitski E, Spies JA, Pan Z, Mao J, Xin HL, Schmuttenmaer CA, Hu S, Kim J-H (2019) Electronic tuning of metal nanoparticles for highly efficient photocatalytic hydrogen peroxide production. ACS Catal 9:626–631
68. Kim K, Park J, Kim H, Jung GY, Kim M-G (2019) Solid-phase photocatalysts: physical vapor deposition of Au nanoislands on porous TiO_2 films for millimolar H_2O_2 production within a few minutes. ACS Catal 9:9206–9211
69. Zheng L, Su H, Zhang J, Walekar LS, Molamahmood HV, Zhou B, Long M, Hua YH (2018) Highly selective photocatalytic production of H_2O_2 on sulfur and nitrogen co-doped graphene quantum dots tuned TiO_2. Appl Catal B 239:475–484
70. Zheng L, Zhang J, Hu YH, Long M (2019) Enhanced photocatalytic production of H_2O_2 by nafion coatings on S, N-codoped graphene-quantum-dots-modified TiO_2. J Phys Chem C 123:13693–13701
71. Ma R, Wang L, Wang H, Liu Z, Xing M, Zhu L, Meng X, Xiao F-S (2019) Solid acids accelerate the photocatalytic hydrogen peroxide synthesis over a hybrid catalyst of titania nanotube with carbon dot. Appl Catal B 244:594–603
72. Isaka Y, Kawase Y, Kuwahara Y, Mori K, Yamashita H (2019) Two-phase system utilizing hydrophobic metal-organic frameworks (MOFs) for photocatalytic synthesis of hydrogen peroxide. Angew Chem Int Ed 58:5402–5406
73. Kawase Y, Isaka Y, Kuwahara Y, Mori K, Yamashita H (2019) Ti cluster-alkylated hydrophobic MOFs for photocatalytic production of hydrogen peroxide in two-phase systems. Chem Commun 55:6743–6746
74. Hayes JA, Schubert DM, Amonette JE, Nachimuthu P, Disselkamp RS (2008) Ultraviolet stimulation of hydrogen peroxide production using aminoindazole, diaminopyridine, and phenylenediamine solid polymer complexes of Zn(II). J Photoch Photobio A 197:245–252
75. Hoffman AJ, Carraway ER, Hoffmann MR (1994) Photocatalytic production of H_2O_2 and organic peroxides on quantum-sized semiconductor colloids. Environ Sci Technol 28:776–785
76. Lu Y, Huang Y, Zhang Y, Huang T, Li H, Cao J-j, Ho W (2019) Effects of H_2O_2 generation over visible light-responsive Bi/$Bi_2O_{2-x}CO_3$ nanosheets on their photocatalytic NO_x removal performance. Chem Eng J 363:374–382
77. Gogoi S, Karak N (2017) Solar-driven hydrogen peroxide production using polymer-supported carbon dots as heterogeneous catalyst. Nano-Micro Lett 9:40